SIMULATION OF SEDIMENT EROSION USING DEM-DPM

Nurhanani A Aziz[1,*], M H Zawawi[1], Aizat Mazlan[1], N H Hassan[1], W N Yusairah[1], F Nurhikmah[1], Aisyahirah Melan[1], Aizat Abas[2], Aqil Azman[2], Muhammad Naqib Nashrudin[2]

[1]*Department of Civil Engineering, Universiti Tenaga Nasional, 43000 Kajang, Selangor, Malaysia*

[2]*School of Mechanical Engineering, Universiti Sains Malaysia, 14300 Parit Buntar, Pulau Pinang, Malaysia*

[*]For correspondence; Tel. + (60) 133690805, E-mail: nurhanani_abdaziz@yahoo.com

ABSTRACT: *Coastal erosion is a natural phenomenon that occurs on the worldwide site of the coastal bank. The impact of natural forces such as wind and waves can change the formation of the shoreline and leads to coastal erosion. Eventually, this work is aimed to conduct a simulation of sediment erosion by using the Discrete Element Method-Discrete Particle Method (DEM-DPM). The simulation works reported that the number of particles changes as the time increase due to the generation of waves. Furthermore, the most critical division can be determined through this simulation as the number of particles starts to change from its initial state. It is also found that the lengthen of time would generally increase the number of particles erode and change the sand formation that will lead to erosion. In addition, the findings have been validated with the Smooth Particle Hydrodynamics method to investigate the effectiveness and accuracy of the numerical analysis of DEM-DPM. Based on the findings, Division A is the most critical division since the particle on that division is erode due to the behaviour of the waves.*

Keywords: Coastal Erosion, DEM, DPM, DEM-DPM.

1. INTRODUCTION

Coastal bank is a most imperative financial locale that able to support satisfaction of human nature, but this region always beneath frequent threat from different natural and man actuated threats including coastal erosion and shoreline scouring [1]. Coastal erosion is one of the natural phenomena that influence a large number of coastal bank sites worldwide [1-10]. Storminess and endless sea-level rise have become a major problem towards the coastal erosion along with a worldwide increment in coastal advancement of numerous nations [10]. Coastal management dealing with erosion complication and long term coastline stability essentially depends on the balance between the rate of sediment supply and transport [11].

Due to the action of waves, beach and shallow water sediments are continuously responding to the action causing erosion and affecting the dynamic equilibrium of the coastal bank [12]. This phenomenon is not only induced by unexpected and extraordinary ocean storms, but it is the result of the natural behavior and persistent impact of the wave affecting the coastline [2]. In addition, the impact of the wave towards the shoreline and the resultant erosion rely on a few aspects such as the strength, the action time, the type of soil and the direction of propagation [2]. Numerous coastal preservation and protection measures have been applied for the improvement and rehabilitation of the coastal bank, but the destructive aftermath of erosion still continues [8]. In order to build or create new coastal protection, it is important to investigate more about the behaviour of the wave towards sand sediment to understand the nature of this erosion. This paper will discuss more the simulation of the sediment erosion using DEM-DPM method.

2. NUMERICAL MODEL

The equation for the conservation of the continuity equation can be composed as shown [13]:

$$\frac{\partial \rho}{\partial t} + \nabla \cdot (\rho \vec{v}) = S_m \qquad (1)$$

Equation (1) is the general form of the mass conservation equation and can be utilized for compressible and incompressible flows. S_m is the mass included in the continuous phase from the dispersed second phase and any user-defined sources.

Conservation of momentum can be described by

$$\frac{\partial}{\partial t}(\rho \vec{v}) + \nabla \cdot (\rho \vec{v} \vec{v}) = -\nabla p + \rho \vec{g} + \vec{F} \qquad (2)$$

Where p is the static pressure and $\rho \vec{g}$ and $\vec{F}$ are the gravitational body force and external body forces respectively. $\vec{F}$ also contains other model-dependent source terms such as porous-media and user-defined sources.

Conservation of energy is expressed by

$$\frac{\partial}{\partial t}(\rho E) + \nabla \cdot [\vec{v}(\rho E + p)] = -\nabla \cdot \left(\sum_j h_j J_j \right) + S_h \qquad (1)$$

2.1 Volume of Fluid (VOF)

Momentum Equation for volume of fluid [13] is given as

$$\frac{\partial}{\partial t}(\rho \vec{v}) + \nabla \cdot (\rho \vec{v} \vec{v}) = -\nabla p + \nabla \cdot [\mu(\nabla \vec{v} + \vec{v}^T)] + \rho \vec{g} + \vec{F} \qquad (4)$$

The energy equation is shown below.

$$\frac{\partial}{\partial t}(\rho E) + \nabla \cdot \left(\vec{v}(\rho E + p)\right) = \nabla \cdot \left(k_{eff} \nabla T\right) + S_h \qquad (5)$$

The VOF model treats energy, E and temperature, T as mass-averaged variables:

$$E = \frac{\sum_{q=1}^{n} \alpha_q \rho_q E_q}{\sum_{q=1}^{n} \alpha_q \rho_q} \qquad (6)$$

Where E_q for each phase is based on the specific heat of that phase and the shared temperature.

2.1.1 Airy Wave Theory

The wave profile for the linear wave is shown below

$$\zeta(X, t) = A \cos \alpha \qquad (7)$$

Where

$$\alpha = k_x x + k_y y - \omega_e t + \varepsilon \quad (8)$$

x and *y* are the space coordinates in the $\hat{x}$ and $\hat{y}$ directions respectively while ε is the phase difference, and *t* is the time.

For both shallow and intermediate waves, the wave frequency ω is defined as given below:

$$\omega = \sqrt{gk\tanh(kh)} \quad (9)$$

And for short gravity waves:

$$\omega = \sqrt{gk} \quad (10)$$

Where *h* is the height of the liquid, *k* is a number of a wave, and *g* is the gravity magnitude.

2.1.2 Stokes Wave Theory

Based on the work by John D. Fenton [13], the Stokes wave theories in fluent is formulated [13]. These theories can be used for large steepness finite amplitudes waves operating in intermediate to deep liquid depth range.

For higher-order Stokes theories (second to fifth order), the generalized expression for wave profiles is shown as:

$$\zeta(X,t) = \frac{1}{k}\sum_{i=1}^{n}\sum_{j=1}^{i} b_{ij}\xi^i \cos(j\alpha) \quad (11)$$

The generalized expression for associated velocity potential is shown as:

$$\Phi(X,t) = \frac{1}{k}\sqrt{\frac{g}{k}\tanh(kh)}\sum_{i=1}^{n}\xi^i\sum_{j=1}^{i} a_{ij}\cosh(\mathrm{jk(z} + \mathrm{h))}\cos(j\alpha) \quad (12)$$

Where,

$$\xi = \frac{kH}{2} \quad (13)$$

ξ is referred to wave steepness.

n = wave theory index (2 to 5: From 2nd order Stokes to 5th order Stokes respectively.

Wave celerity, *c* is given as;

$$c = \sqrt{\frac{g}{k}\tanh(kh)}\,(1 + c_3\xi^2 + c_5\xi^4) \quad (14)$$

For 2nd order Stokes, $c_3 = c_5 = 0$, while for 3rd and 4th order Stokes, $c_5 = 0$.

Wave frequency, ω, is defined as

$$\omega = kc \quad (15)$$

Velocity components for surface gravity waves are derived from the velocity potential function.

$$u = \frac{\partial\Phi}{\partial x}\cos\theta \quad (16)$$

$$v = \frac{\partial\Phi}{\partial x}\sin\theta \quad (17)$$

$$w = \frac{\partial\Phi}{\partial x}\tan\theta \quad (18)$$

2.2 Discrete Particle Model

Each particle is tracked individually in a Euler-Langrangian model by using Newton's second law of motion [14], given by

$$m_{\mathrm{p}}\frac{\mathrm{d}\vec{v}_p}{dt} = m_{\mathrm{p}}\vec{\mathrm{g}} + \frac{V_p\beta}{1-\epsilon}\left(\vec{u} - \vec{v}_p\right) - V_p\nabla p \quad (19)$$

The fluid phase hydrodynamics are described with the continuity equation and the volume-averaged Navier-Stokes equations [14]:

$$\frac{\partial(\epsilon\rho_{\mathrm{f}})}{\partial \mathrm{t}} + \nabla\cdot\epsilon\rho_{\mathrm{f}}\vec{u} = 0 \quad (20)$$

$$\frac{\partial(\epsilon\rho_{\mathrm{f}}\vec{u})}{\partial \mathrm{t}} + \nabla\cdot\epsilon\rho_{\mathrm{f}}\vec{u}\vec{u} = -\epsilon\nabla p - \nabla\cdot\epsilon\vec{\tau}_f - \vec{S}_p + \epsilon\rho_{\mathrm{f}}\vec{\mathrm{g}} \quad (21)$$

Where $\vec{S}_p$ is the source term that accounts for the momentum exchange between the fluid phase and the particle phase. $\vec{S}_p$ can be calculated as below:

$$\vec{S}_p = \frac{1}{V}\int\sum_{k=0}^{N_p}\frac{V_{p,k}\beta}{1-\epsilon}\left(\vec{u} - \vec{v}_{p,k}\right)\delta\left(\vec{r} - \vec{r}_{p,k}\right)dV \quad (22)$$

The δ-function is to ensure that the reaction force acts as a point force at the position of the particle in the system.

2.2 Discrete Element Method (DEM)

The implementation of DEM is based on [15], and accounts for the forces that result from the collision of the particles. Discrete Element Method (DEM) is a common computational technique introduced by [15] to model the dynamics of granular matter such as gravel, coal, beads of any material. It involves trajectories and spins of all particles and objects in the system and able to predict their interactions with other particles and with their environment [16]. DEM simulation can be characterized by a high volume fraction of particles, where interaction between particles is important [13].

2.2.1 The Spring-Dashpot Collision Law

In spring-dashpot collision law, a spring constant *K* can be defined as in the spring collision law, along with a coefficient of restitution for the dashpot term (η) which $0 < \eta \leq 1$.

The following equation is evaluated in preparation for the calculations of force:

$$f_{loss} = \sqrt{\pi^2 + \ln^2\eta} \quad (23)$$

$$m_{12} = \frac{m_1 m_2}{m_1 + m_2} \quad (24)$$

$$t_{coll} = f_{loss}\sqrt{\frac{m_{12}}{K}} \quad (25)$$

$$\gamma = -2\frac{m_{12}\ln\eta}{t_{coll}} \quad (26)$$

$$\vec{v}_{12} = \vec{v}_2 - \vec{v}_1 \quad (27)$$

Where f_{loss} is the loss factor. m_1 and m_2 are the masses of particle 1 and 2 respectively while m_{12} is the 'reduce mass' . t_{coll} is the collision time scale, $\vec{v}_1$ and $\vec{v}_2$ are the velocities of particles 1 and 2 respectively, while $\vec{v}_{12}$ is the relative velocity. γ is the damping coefficient, and $\gamma \geq 0$ because of $\ln \eta \leq 0$.

The force on particle 1 can be calculated as below;

$$\vec{F}_1 = \left(K\delta + \gamma(\vec{v}_{12} \cdot \vec{e}_{12})\right)\vec{e}_{12} \qquad (28)$$

By Newton's third law, the force on particle 2 is given as

$$\vec{F}_2 = -\vec{F}_1 \qquad (29)$$

3. RESULTS AND DISCUSSION

3.1 Volume Fraction

Figure (1) illustrates the volume fraction of the seawater together with sand particles at a different time step. It can be observed that the seawater at initial position is stable as the seawater just fill up the model and after few seconds, the generation of the wave can be seen in Figure (1, b, c, d, e) since the seawater is not stable just like at the initial position. Whenever those phenomena occur, the sand particles start to change their initial state and have been transporting to other places. With the help of the drag force, the particles will move slowly towards the direction of the incoming wave and lead the particles to erode.

In the beginning of generation, the sand particles are full within the sediment boundary before the presence of waves as shown in Figure (1, a). The sand particles at the upper part of the sediment boundary start to erode and having gaps after a few seconds. This phenomenon happens because of the wave behaviour that acts towards the sediment boundary and changes the sand formation. Based on Figure (1 a,b,c,d,e), the gaps between sand particles at the upper part of sediment boundary are increasing as the time increase.

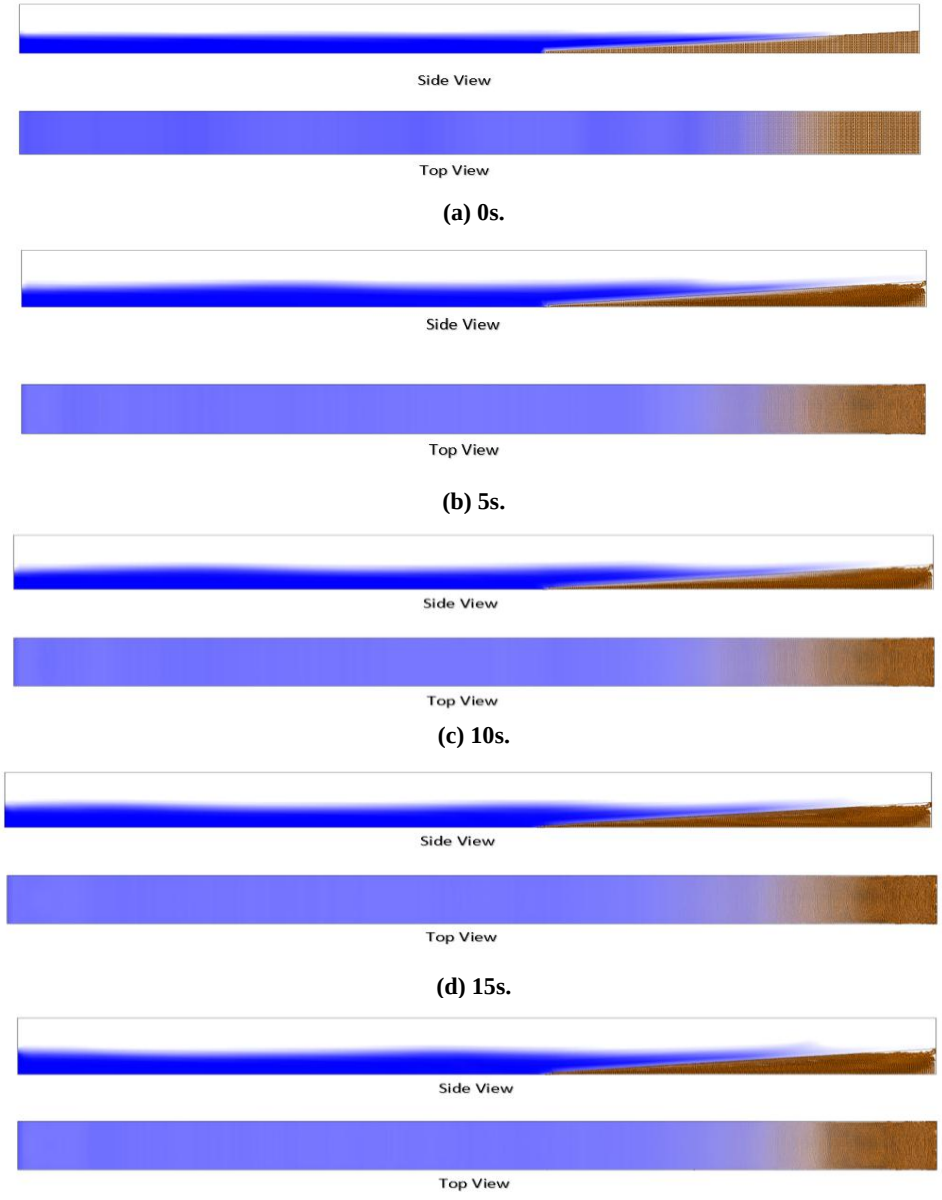

Figure (1) Movement of Waves and Sand

3.2 Number of Particles

The division of the sediment boundary, the number of particles in each division and the changes of particles over time are shown in Figure (2), Table (1) and Table (2) simultaneously. Through this division, the change of the number of sand particles can be investigated to determine the most critical division that has a high risk for erosion to occur. The number of particles can be determined by the particle file that has been injected during the simulation is conducted. The particle files consist of particle size and the gap or distance between particle and particle. Hence, the most critical division can be determined by the changes in particle number as the time is increasing.

Figure (2) The Division of Sediment Boundary.

Table (1) show the number of particles in each division. The number of particles at the initial position is different for each division as the volume of each part is different. Division A has a bigger number of particles with 55,152 while division C has a smaller number of particles with 14,472. As the simulation is conducted, the number of particles in each division starts to change due to the behaviour of the wave.

Table (1) The number of particles in each division.

Number of Particles					
Division / Time	0s	5s	10s	15s	20s
A	55,152	54,342	53,694	53,142	52,673
B	34,272	34,844	35,210	35,457	35,517
C	14,472	14,642	14,888	15,159	15,542

Based on Table (1) and Table (2) the number of particles in division A is decreasing as the time increase. The number of particles for division A starts with 55,152 and drop to 52,673 after the 20s. While in division B and C, the number of particles is increasing when the time is increasing. The number of particles for division B and C starts with 34,272 and 14,472 then increases to 35,517 and 15,542 simultaneously after the 20s.

This phenomenon happens because of the drag force that acts towards the sediment boundary. The particles from the upper part (division A) had been drag by the waves towards the division B and C. Therefore, the number of particles in division A is decreasing while in division B and C in increasing. Based on Table (1) and Table (2), we can conclude that the most critical division between these three divisions is division A since this division lost a lot of the number of particles compare to other divisions.

Table (2) Changes in the number of particles over time.

Change of Particles				
Division / Time	$T_0 - T_5$	$T_5 - T_{10}$	$T_{10} - T_{15}$	$T_{15} - T_{20}$
A	-810	-648	-552	-469
B	572	366	247	60
C	170	246	271	383

3.3 Validation

To investigate the effectiveness and the accuracy of the numerical analysis of DEM-DPM, the validation with another method which is Smooth Particle Hydrodynamics (SPH) should be made. The same model is used for both methods to compare and validate the results. However, the results of these two methods are slightly different due to the mesh used. DEM-DPM is a numerical analysis that needed mesh to conduct the analysis while SPH is meshed free.

The validation of the two methods is shown in Figure (3). Based on the figure, the pattern of the particle erode is slightly the same between these two methods. For both methods, the particle erodes occur at the same area which is at the upper part of the sediment boundary (Division A). The particle erodes from the upper part because the particle is dragged by the drag force of the wave and move downwards to the lower part followed the direction of the incoming wave.

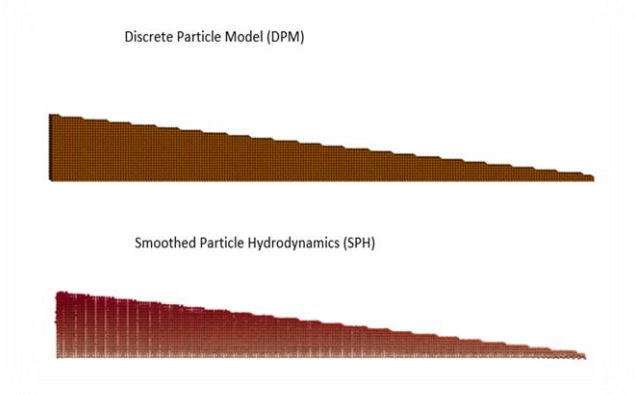

(a) 0s

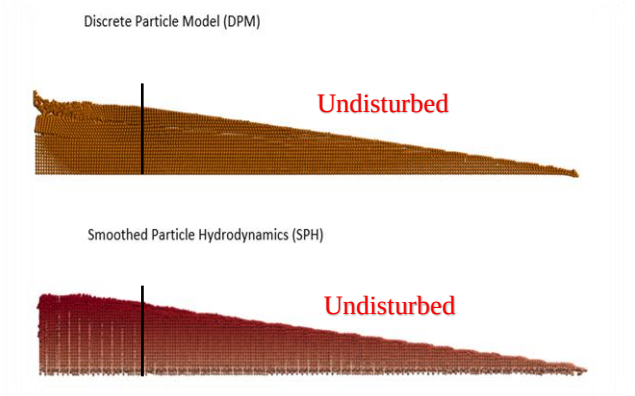

(b) 5s

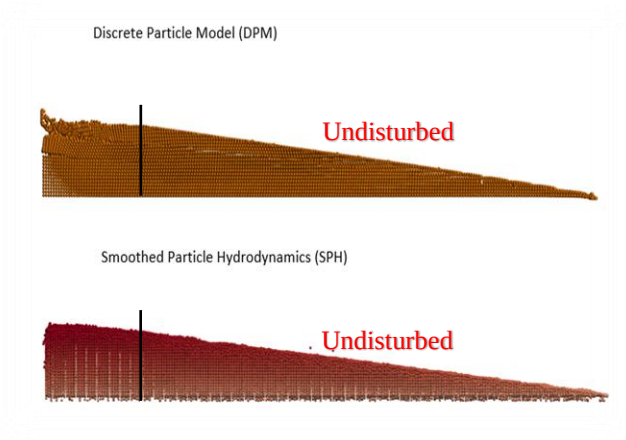

(c) 10s

Figure (3) Validation between two methods.

4. CONCLUSION

The sediment erosion has been successfully simulated numerically using a DEM-DPM method. Accordingly, we presumed that the findings were validated based on the SPH method as the pattern of the particle erode are the same for both methods. It is also found that the lengthen of time would generally increase the number of particles erode and change the sand formation that will lead to erosion. For instance, the number of particle for the upper part of the sediment boundary (part A) keep on decreasing as the time increase while in other parts (part B and C), the number of particles keep on increasing due to the loss of particles in part A. Therefore, this will indicate that part A has a high possibility for the erosion to occur due to wave behaviour.

5. ACKNOWLEDGEMENT

This research project was funded by the Tenaga Nasional Berhad seeding fund under grant No. U-TG-RD-18-05.

6. REFERENCE

[1] A. V. Hegde and B. J. Akshaya, "Shoreline Transformation Study of Karnataka Coast : Geospatial Approach," *Aquat. Procedia*, vol. 4, no. Icwrcoe, pp. 151–156, 2015.

[2] F. Adamo, C. De Capua, P. Filianoti, A. M. L. Lanzolla, and R. Morello, "A coastal erosion model to predict shoreline changes," *Meas. J. Int. Meas. Confed.*, vol. 47, no. 1, pp. 734–740, 2014.

[3] M. R. R. M. A. Zainol, M. A. Kamaruddin, M. H. Zawawi, and K. A. Wahab, "Numerical Analysis Study of Sarawak Barrage River Bed Erosion and Scouring by Using Smooth Particle Hydrodynamic (SPH) Numerical Analysis Study of Sarawak Barrage River Bed Erosion and Scouring by Using Smooth Particle Hydrodynamic (SPH)," *Mater. Sci. Eng.*, vol. 267, 2017.

[4] M. Sedigh, R. Tomlinson, N. Cartwright, and A. Etemad-Shahidi, "Numerical modelling of the Gold Coast Seaway area hydrodynamics and littoral drift," *Ocean Eng.*, vol. 121, pp. 47–61, 2016.

[5] M. Besset, E. J. Anthony, P. Dussouillez, and M. Goichot, "The impact of Cyclone Nargis on the Ayeyarwady (Irrawaddy) River delta shoreline and nearshore zone (Myanmar): Towards degraded delta resilience?," *Comptes rendus - Geosci.*, vol. 349, no. 6–7, pp. 238–247, 2017.

[6] J. M. Zhang, J. H. Zhang, G. Wang, and Y. Chen, "Safety evaluation of breakwaters based on physical and numerical modelling," *Ocean Eng.*, vol. 36, no. 11, pp. 852–862, 2009.

[7] P. K. Mohanty, S. K. Barik, P. K. Kar, and B. Behera, "Impacts of Ports on shoreline change along Odisha coast," *Procedia Eng.*, vol. 116, no. Apac, pp. 647–654, 2015.

[8] V. Noujas, K. V. Thomas, and N. R. Ajeesh, "Shoreline management plan for a protected but eroding coast along the southwest coast of India," *Int. J. Sediment Res.*, vol. 32, no. 4, pp. 495–505, 2017.

[9] H. Burningham and J. French, "Understanding coastal change using shoreline trend analysis supported by cluster-based segmentation," *Geomorphology*, vol. 282, pp. 131–149, 2017.

[10] C. Adriana Gracia, N. Rangel-Buitrago, J. A. Oakley, and A. Williams, "Use of ecosystems in coastal erosion management," *Ocean Coast. Manag.*, vol. 156, pp. 277–289, 2017.

[11] M. Bahgat, "Optimum use of dredged materials for sustainable shoreline management in Nile Delta," *Water Sci.*, pp. 1–14, 2017.

[12] K. Jyothi, J. S. Mani, and M. R. Pranesh, "Numerical modelling of flow around coastal structures and scour prediction," *Ocean Eng.*, vol. 29, no. 4, pp. 417–444, 2001.

[13] ANSYS Inc., "ANSYS Fluent Theory Guide," *ANSYS Inc., USA*, vol. 15317, no. August, pp. 724–746, 2016.

[14] G. A. Bokkers, M. Van Sint Annaland, and J. A. M. Kuipers, "Mixing and segregation in a bidisperse gas-solid fluidised bed: A numerical and experimental study," *Powder Technol.*, vol. 140, no. 3, pp. 176–186, 2004.

[15] P. A. Cundall and O. D. L. Strack, "A discrete numerical model for granular assemblies," *Géotechnique*, vol. 29, no. 1, pp. 47–65, 1979.

[16] J. Hurley, N. Stokes, and P. W. Cleary, "Efficient collision detection for three dimensional super-ellipsoid particles," *Proc. 8th Int. Comput. Tech. Appl. Conf.*, no. January 1997, pp. 1–7, 199

*For correspondence; Tel. + (60) 133690805, E-mail:nurhanani_abdaziz@yahoo.com